AIChE

Inclination Effects on Wave Characteristics in Annular Gas–Liquid Flows

A. Al-Sarkhi
Dept. of Mechanical Engineering, King Fahd University of Petroleum & Minerals, Dhahran, Saudi Arabia

C. Sarica and K. Magrini
Dept. of Petroleum Engineering, The University of Tulsa, Tulsa, OK 74104

DOI 10.1002/aic.12653
Published online May 9, 2011 in Wiley Online Library (wileyonlinelibrary.com).

Measurements of wave characteristics have been conducted in a 0.0762 m internal diameter (ID) pipe at inclinations of 0°, 10°, 20°, 45°, 60°, 75°, and 90° from horizontal. Wave celerity and frequency are very strongly dependent on modified Lockhart–Martinelli parameter, X*, *and the inclination angle. Wave amplitude increases with increasing liquid film thickness at the bottom of the pipe. Wave amplitude depends on liquid film thickness for any pipe diameter, surface tension, and viscosity. Strouhal number (dimensionless wave frequency) decreases with increasing* X*. *Effect of pipe diameter, surface tension, and liquid viscosity on the liquid film Reynolds number,* Re_{LF}, *was studied.* Re_{LF} *variation with* X* *is not sensitive to the surface tension and less sensitive to the pipe diameter. However,* Re_{LF} *is very sensitive to the viscosity of the flowing liquid. Correlations for wave celerity, amplitude, frequency, and liquid film Reynolds number are proposed.* © 2011 American Institute of Chemical Engineers *AIChE J,* 58: 1018–1029, 2012
Keywords: annular flow, wave characteristics, pipe inclination, fluid mechanics, multiphase flow

Introduction

An annular flow pattern can exist at high gas velocities in a pipe. In annular flow, liquid flows in a film along the pipe wall and as droplets entrained in the gas core. There is a liquid mass transfer between the film and the gas core, whereby droplets deposit at the film and are formed by atomization at the film–gas core interface. Because of gravity, the liquid film at the wall is distributed asymmetrically for all configurations except vertical. For air–water systems, the flow in the film is characterized by the intermittent appearance of disturbances, which are a group of large amplitude waves that could be considered as patches of turbulence. The irregular waves are the source of drops that enter the gas phase.

Correspondence concerning this article should be addressed to A. Al-Sarkhi at alsarkhi@kfupm.edu.sa.

The annular flow pattern is quite different for small diameter pipes [less than 3 cm internal diameter (ID)] and large diameter pipes (larger than 5 cm ID) in that the disturbance waves for small diameter pipes are wrapped around the whole circumference. The pattern resembles what is observed in vertical pipes.[1]

Geraci et al.[2] explained how the majority of drops in annular flow are created from the wall film by the action of flowing of the gas phase over it. However, drops are not created from the entire liquid film interface, but particularly they arise from disturbance waves.

Azzopardi and Whalley[3] concluded that waves are the source of drops. This conclusion was proved through the experiment in which injecting small quantities of liquid into a film flow whose flow rate was just below the flow rate for the formation of waves, they were able to create waves on demand. These experiments, which used an axial viewing

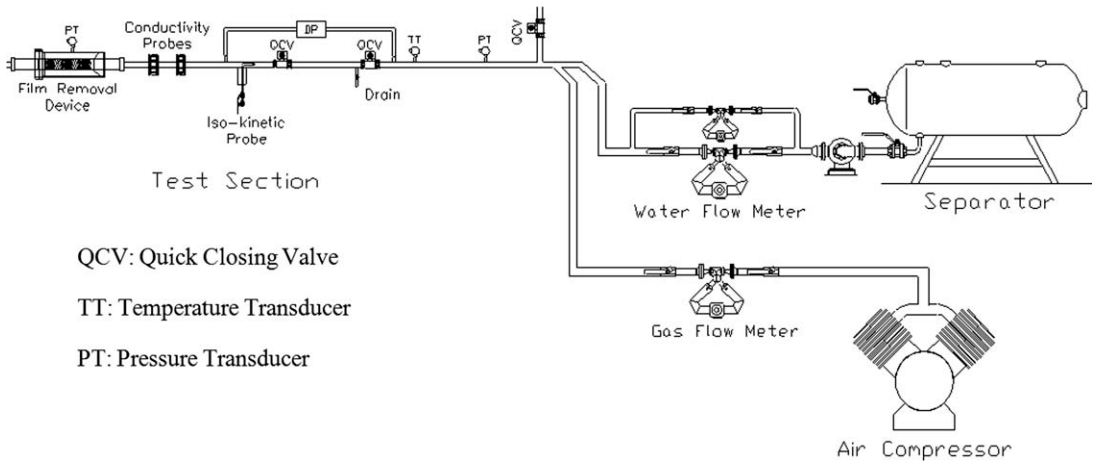

Figure 1. Schematic of the test facility.

technique, gave very strong proof that drops are only created when waves are present.

Sutharshan et al.[4] measured the liquid film velocity in horizontal annular flow in a pipe with 0.0254 m ID. It was concluded that the liquid is transported to the upper part of the tube against the force of gravity by the disturbance waves and not by the secondary gas flow or any other mechanisms.

Geraci et al.[5] studied the effect of inclination on the disturbance wave characteristics in 38 mm pipe diameter. It was observed that in horizontal flow, the film interface is covered by large disturbance waves only over the lower half of the pipe, whereas at the top, there are only small amplitude ripples. With increasing the inclination of the pipe upward from the horizontal, the amplitude of the disturbance waves decreases, but the fraction of the pipe circumference over which disturbance waves occur increases. At inclinations very close to vertical, disturbance waves are present around the entire section.

The influence of entrained droplets in horizontal annular flows is more complicated than that of the vertical orientation. The wave characteristics and liquid film distribution in horizontal or slightly inclined pipes are different from those in vertical or highly inclined pipes. The rate of droplet deposition varies with gravitational settling that causes an asymmetric distribution of droplets/film thickness and contributes directly to the local rate of deposition. The influence of gravity on deposition and the asymmetric distribution of drops increases with increasing droplet size and pipe inclination from vertical to the horizontal orientation.

Entrainment occurs by the breaking up of the interfacial waves.[6] The description of the wave characteristics, namely, celerity, wavelength, frequency, and amplitude are very important for prediction and modeling the droplet entrainment. The onset of entrainment is strongly dependent on the wave celerity and amplitude.[7] Wave modeling deals with the prediction of the conditions at which waves are formed and become unstable. In the past, several studies of the wave characteristics based on the linear stability analysis have been obtained.[8–13] Several other studies have been attempted with nonlinear analysis and shallow water theory.[14–18]

The entrainment fraction is strongly related to the waves taking place at the gas–liquid interface. There is a large amount of data and correlations for the prediction of entrainment fraction in literature. However, the entrainment predictions vary significantly with the different correlations resulting in high uncertainties, which affect any calculation and design that include entrainment. The correlations, mostly, do not incorporate wave characteristics, which affect significantly the entrainment fraction.[19] In addition, there is a lack of a complete mechanistic model with good confidence level for the prediction of entrainment fraction.

The present study differs from the previous work on wave characteristics in annular flows in that a larger pipe diameter was used, a more careful study of the effect of inclination angle from horizontal to vertical was carried out and the influence of the pipe inclination angles on the wave characteristics was identified.

The focus of this article is to examine the effect of pipe inclination and diameter on wave characteristics in annular flows. The present results were compared with Mantilla[19] and Mantilla et al.[20] at different pipe diameters for the horizontal case. This information is critically important in predicting the behavior of an annular flow and fraction of entrainment prediction in large diameter pipes.

Experimental Setup and Procedure

Experimental facility

A schematic of the test facility is shown in Figure 1. The 76.2-mm ID facility is 17.5 m long and is inclinable from 0° to 90° from horizontal. Air and water were used as the working fluids. At standard conditions, the water density, viscosity, and surface tension are 998 kg/m^3, 0.001 Pa s, and 0.073 N/m, respectively. The compressed air was supplied by dry rotary screw and two-stage compressors. Both gas and liquid were metered using Coriolis type mass flow meters. The water is pumped using a progressive cavity pump. Both the air and water are relieved to atmosphere at the outlet of the pipe section to decrease the back pressure of the system and increase air velocities. The gate valve of 76.2-mm is located at the outlet to control the back pressure of the system. The test section consisted of three major components: a quick-closing valve section, film removal section, and conductivity probe section.

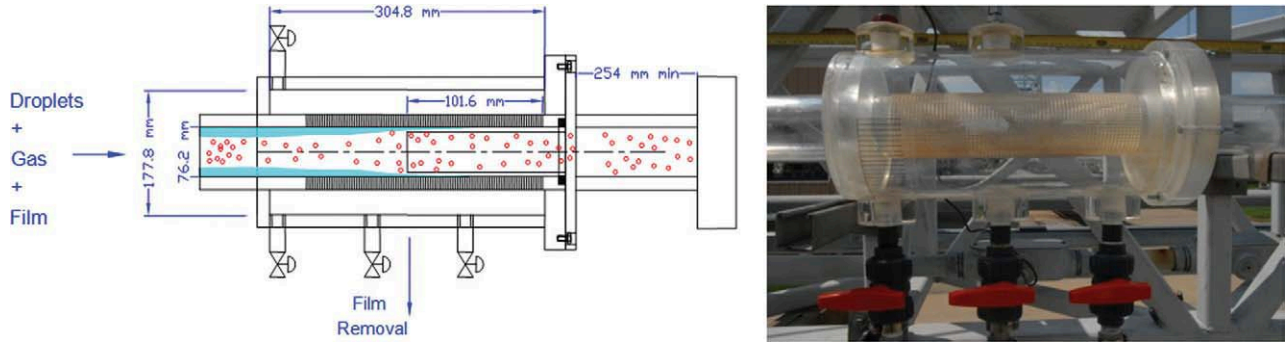

Figure 2. Film removal device.

[Color figure can be viewed in the online issue, which is available at wileyonlinelibrary.com.]

Table 1. Test Matrix and Cases Studied

	Group 1					Group 2					Group 3					Group 4				
Case	1	2	3	4	5	6	7	8	9	10	11	12	13	14	15	16	17	18	19	20
V_{SL} (m/s)	0.0035	0.0035	0.0035	0.0035	0.0035	0.01	0.01	0.01	0.01	0.01	0.02	0.02	0.02	0.02	0.02	0.04	0.04	0.04	0.04	0.04
V_{SG} (m/s)	40	50	60	70	80	40	50	60	70	80	40	50	60	70	80	40	50	60	70	80

Film removal section

The film removal section is located 13-m (L/D = 172) downstream of the inlet. The section consists of a film removal device and film volume tank. The film removal device is used to measure the liquid film flow rate. The device utilizes a long porous section and inserted sleeve to separate the liquid film from the entrained droplets. Figure 2 is a schematic and a picture of the film removal device. The flow passes through the porous section and the liquid film, traveling at a lower velocity than the gas core, is pushed through the porous section. The high inertia of the entrained droplets, flowing close to the gas velocity, prevents them from being removed through the porous section. To ensure no droplets will escape, a long sleeve was inserted close to where the liquid film dissipates. This sleeve is able to move in and out in the pipe to make sure the liquid film passes under the sleeve and only the gas core with droplets passes through the test section. The film volume is collected in a small tank with a capacity of 22 l. The volume of water from the liquid film and sampling time (10 min) are measured to determine the film flow rate. The measurement is repeated three times for each test point to ensure the accuracy of the results.

Experimental range

One hundred and forty annular two-phase flow tests were conducted for inclination angles of 0°, 10°, 20°, 45°, 60°, 75°, and 90° from horizontal. The test matrix conducted for each angle in this work is shown in Table 1. For each test, the pressure at the film removal device is held constant using the gate valve at the outlet of the pipe. In addition, both liquid and gas flow rates are held constant for each experimental run. In Table 1, every group has common superficial liquid velocity, V_{SL}; every case has the same superficial liquid and gas velocity and variable inclination angle from 0° to 90°.

Conductivity probe section

The conductivity section is utilized to obtain average thickness and wave characteristics of the liquid film. Located 12.5-m (L/D = 164) from the inlet, the conductivity probe section consists of two probe assemblies, flush mounted

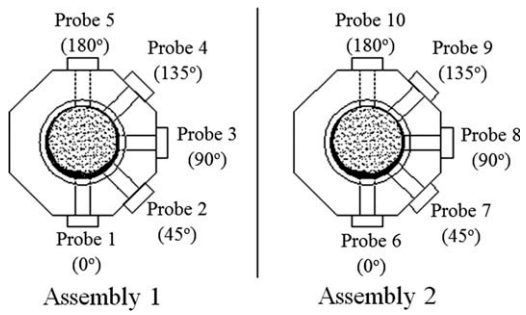

Figure 3. Conductivity assembly setup.

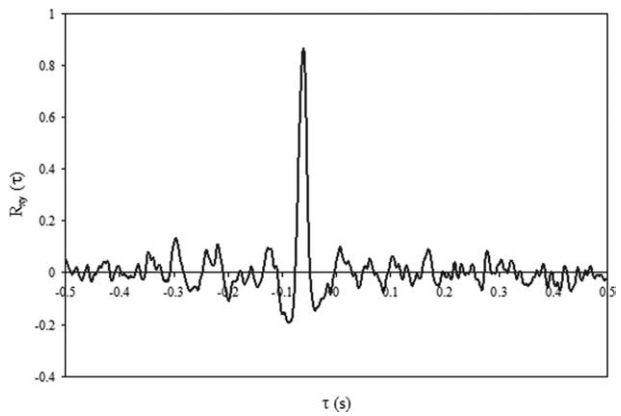

Figure 4. Cross-correlation result example.

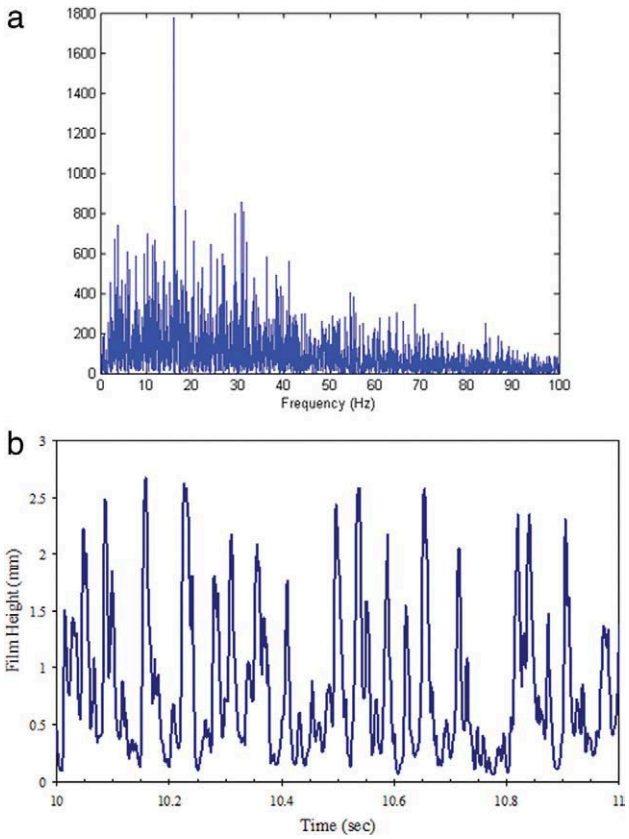

Figure 5. A: MATLAB power spectrum.

B: Liquid film height time trace. [Color figure can be viewed in the online issue, which is available at wileyonlinelibrary.com.]

conductance probes, and a conductivity meter printed circuit board. To obtain the film height, the conductivity meter board applies a DC voltage across the probes and reads the resulting current between the two plates of the probe. This current is then converted to an analog signal. This signal is then recorded by a handheld Omega AD128 data logger at a rate of 500 Hz.

The conductance section consists of two octagonal shaped probe assemblies spaced 0.15 m apart. Each assembly contains five flush mounted probes installed from the bottom to the top of the pipe, spaced 45° apart. The orientation of the probes in each assembly can be found in Figure 3.

Flush mounted conductance probes were chosen for this study because of the thin liquid films encountered at the studied flow conditions. Liquid films from 4-mm down to 0.03-mm can be measured with this probe type. The flush mounted probes consist of two parallel plates, 1.59-mm wide and 10-mm long, spaced 1.5-mm apart. Brass is used in the construction of the probes because of its high conductivity and corrosion resistance.

The flush mounted conductance probes are calibrated dynamically to avoid any complications encountered with static calibration. Flow conditions produce a variation of thick to very thin films were selected to develop the calibration curve. A Fowler depth micrometer model Mark IV with an accuracy of 0.002-mm has been used to determine the true height of the liquid film. The micrometer is attached to a conductivity circuit with one lead in the flowing film and the micrometer tip being used as the second lead. For each superficial gas and liquid velocity, the mean film thickness is found using the micrometer, conductivity circuit, and oscilloscope, more details can be found in Magrini.[21]

Wave measurements

Wave characteristics are recorded simultaneously with the measurement of the liquid film flow rate. Each test is recorded for 40 s at a rate of 500 Hz. The conductivity of the fluid is measured during each test using an YSI conductivity meter model 30.

Quick-closing valves are used to measure the liquid holdup. Because of the low volume of liquid holdup for the given conditions, a syringe is used to extract the liquid.

The film thickness is measured using flush mounted conductivity probes installed from the bottom to the top of the pipe, spaced 45° apart. The average film thickness is determined by averaging a 40-s time trace for each probe.

Wave celerity

The wave celerity is calculated using the cross-correlation between two conductivity probes spaced a known distance apart. The time delay between signals is determined using MATLAB and confirmed with a hand written VBA program in Microsoft Excel. An example of the cross-correlation calculation can be found in Figure 4 for flow conditions of $V_{SL} = 0.04$ m/s and $V_{SG} = 80$ m/s at horizontal.

Table 2. Uncertainty Analysis Results

Parameter	Instrument	Random Uncertainty	Systematic Uncertainty	Combined Uncertainty
Liquid flow rate (%)	Micro motion flow meter	0.23	0.05	0.46
Gas flow rate (%)	Micro motion flow meter	0.37	0.04	0.74
Pressure (%)	Rosemount pressure transmitter	0.41	1.10	1.37
Pressure drop (%)	Rosemount differential pressure transmitter	0.22	1.00	1.10
Temperature (°C)	Rosemount temperature transmitter	0.06	0.5	0.52
Liquid holdup (%)	Quick-closing valve section	1.68	5.60	6.53
Liquid entrainment (%)	Isokinetic sampling system	3.84	5.8	9.58
Liquid film height (mm)	Flush mounted conductance probe	0.015	0.025	0.039
Diameter (%)	–	0.01	0.07	0.07
Gas velocity (%)	–	0.62	1.83	2.21
Liquid velocity (%)	–	0.34	0.76	1.02

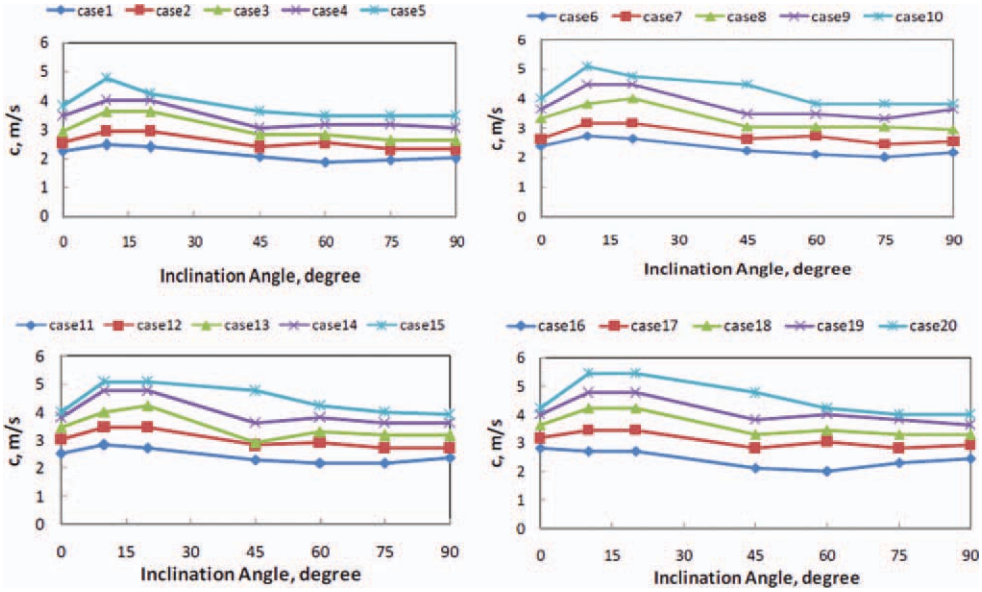

Figure 6. Wave celerity variation with pipe inclination angle at different gas and liquid superficial velocities (cases are listed in Table 1, for each figure or group increasing the number of the case means increasing the V_{SG} at same V_{SL}).

[Color figure can be viewed in the online issue, which is available at wileyonlinelibrary.com.]

Wave frequency

The wave frequency is determined using a combination of the power spectrum method in MATLAB and manual counting of the wave peaks from film holdup time traces. The power spectrum gives the predominant frequency or range of frequencies. The waves are then manually counted and compared with the power spectrum value. For the case of $V_{SL} = 0.04$ m/s and $V_{SG} = 50$ m/s at horizontal, the corresponding power spectrum can be found in Figures 5A, B. The time trace of the film height for the same flowing conditions is shown in Figure 5A. As can be seen in Figure 5B, the predominant frequency is 18 Hz, which matches the number of waves in the time trace.

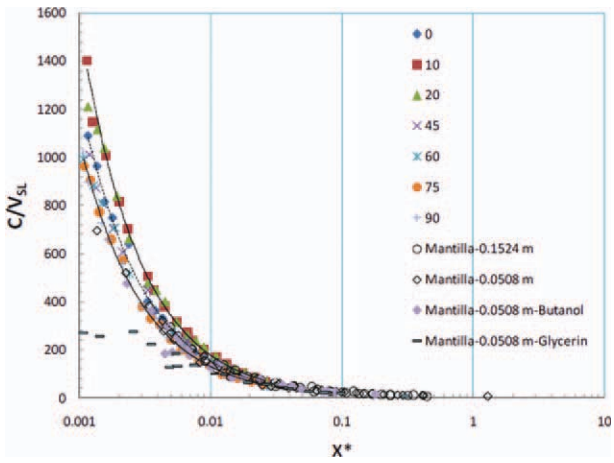

Figure 7. Normalized wave celerity vs. X^* for different pipe inclinations and diameters, and liquid viscosity and surface tension.

[Color figure can be viewed in the online issue, which is available at wileyonlinelibrary.com.]

Wave amplitude

The wave amplitude is determined by averaging the wave heights of a film height time trace that are larger than the average film thickness plus 2 standard deviations.

The uncertainty analysis for the parameters in this study can be found in Table 2.

Results and Discussion

Wave characterization in an annular flow will be explained based on wave celerity, C, frequency, f, and amplitude, $\Delta h_W(0)$ and the liquid film thickness at the bottom of the pipe, $h_L(0)$, the liquid film Reynolds number, Re_{LF}, and liquid film velocity, V_{LF}.

Wave celerity

Wave celerity, C, is a strong function of the superficial liquid, and gas velocities. The celerity is also dependent on the inclination angle. The wave celerity increases with increasing superficial gas and liquid velocities. As can be seen in Figure 6, starting from the horizontal case, wave celerity increases as the pipe is inclined. The wave celerity reaches a maximum point between the 10° and 20° inclination angle. After this maximum, the wave celerity will decrease until it reaches the minimum and approximately constant value near vertical. For constant superficial velocities, the variation in the wave celerity is almost negligible between 70° and 90° of pipe inclination, therefore, the effect of pipe inclination on the wave celerity is substantial over

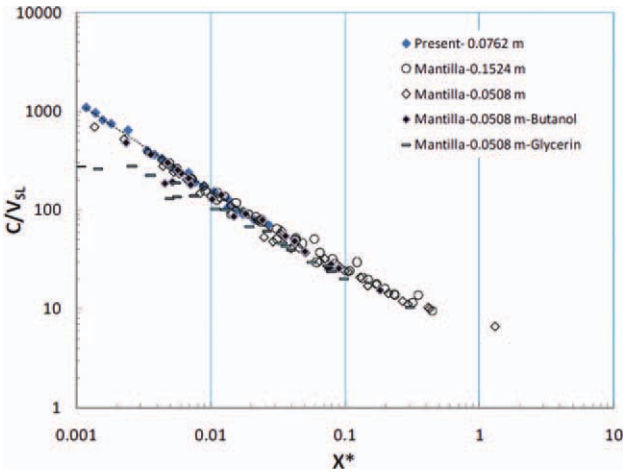

Figure 8. Wave celerity variation with *X in horizontal pipes.**

[Color figure can be viewed in the online issue, which is available at wileyonlinelibrary.com.]

the range of inclinations from 10° to 20° in the range of V_{SL} and V_{SG} of this study.

In general, wave celerity and entrainment fraction are very strongly dependent on modified Lockhart–Martinelli parameter, X^*, or the Froude number ratio based on the superficial liquid and gas velocities and pipe inclination angle. X^* can be defined as

$$X^* = \sqrt{\frac{\rho_G}{\rho_L}}\frac{\dot{m}_L}{\dot{m}_G} = \sqrt{\frac{\rho_L}{\rho_G}}\frac{V_{SL}}{V_{SG}} = \frac{Fr_{SL}}{Fr_{SG}};$$
$$Fr_{SL} = \sqrt{\frac{\rho_L V_{SL}^2}{(\rho_L - \rho_G)gD\cos\theta}};\ Fr_{SG} = \sqrt{\frac{\rho_G V_{SG}^2}{(\rho_L - \rho_G)gD\cos\theta}} \quad (1)$$

Table 3. Properties of Fluids Used in Mantilla[19]

Parameter	Value
Water	
Density (kg/m^3)	997
Viscosity (Pa s)	0.00102
Surface tension (N/m)	0.073
Water–5% butanol	
Density (kg/m^3)	989
Viscosity (Pa s)	0.00122
Surface tension (N/m)	0.035
Water–47% glycerin–salt	
Density (kg/m^3)	1130
Viscosity (Pa s)	0.0071
Surface tension (N/m)	0.061

Al-Sarkhi and Sarica[22] used the parameter X^* for the first time to correlate the multiphase flow pressure drop. X^* is somewhat different from Lockhart–Martinelli parameter. Lockhart and Martinelli[23] related the two-phase flow pressure drop to single-phase pressure drops with Lockhart–Martinelli parameter X_{LM}, where the square of X_{LM} is equal to the ratio of the single-phase pressure drops $\Delta P_l/\Delta P_g$. X^* parameter is similar to $X_{LM}\sqrt{f_g/f_l}$, where f_g and f_l are the single-phase gas and liquid friction factors, respectively. Using X^* for the analysis will combine the ratio of superficial velocities and densities of liquid and gas in a single parameter. Figure 7 shows the wave celerity normalized by the superficial liquid velocity plot against the X^*. Increasing X^* will decrease the C/V_{SL}.

The similarity in the behavior or the grouping of low and high inclination angles can be noticed from Figure 7. It is clearly seen that from 10° to 20° the celerities are higher than the horizontal and the rest of the inclination angles due to the changes in the wave structure within the range of the operational condition of this study. This behavior motivated us to investigate group of low and high angle of inclinations in the analysis of the characteristics of the waves.

The wave celerity can be correlated with very good accuracy for the horizontal, the inclination angles of 10° and

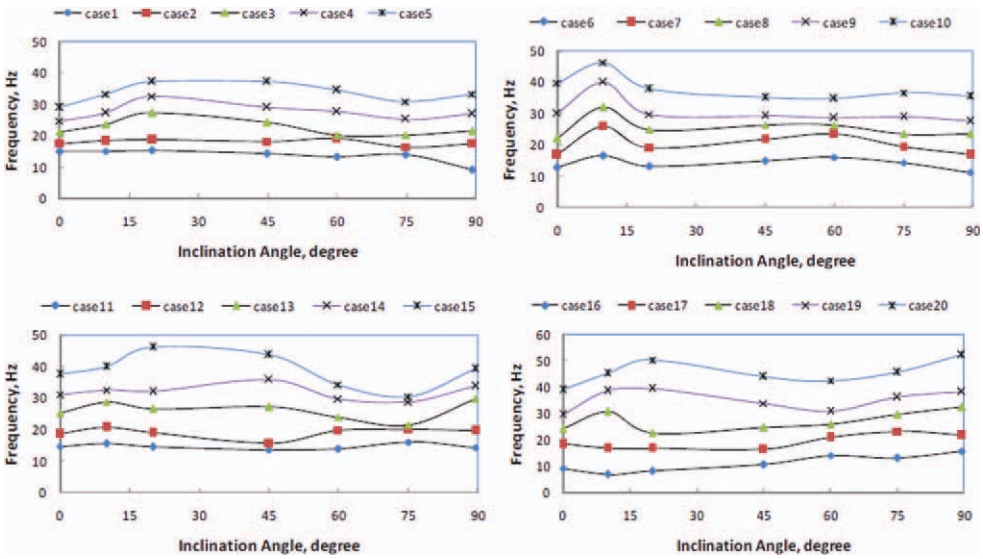

Figure 9. Wave frequency variation with inclination angle.

[Color figure can be viewed in the online issue, which is available at wileyonlinelibrary.com.]

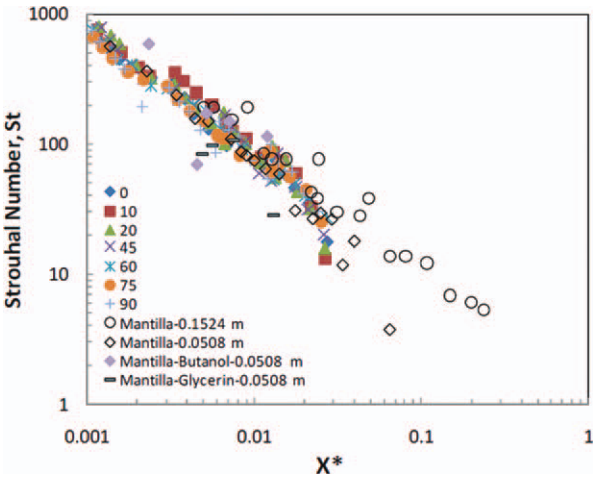

Figure 10. Strouhal number variation with *X.**

[Color figure can be viewed in the online issue, which is available at wileyonlinelibrary.com.]

20°, and the inclination angles of 45° and up to 90° cases, respectively, as

$$C/V_{SL} = 2.379X^{*-0.9} \quad (2)$$

$$C/V_{SL} = 2.323X^{*-0.94} \quad (3)$$

$$C/V_{SL} = 1.942X^{*-0.91} \quad (4)$$

Figure 8 shows the comparison for the horizontal case of the present study and Mantilla.[19] These are different results from different laboratories in different pipe diameters at different viscosity and surface tension. The last case in the legends is for Mantilla[19] for air–water–glycerin–salt has a viscosity of seven times higher than other cases. Almost all cases follow similar behavior except the high viscosity case at low values of *X**. The fluid properties of the fluids used in Mantilla[19] are given in Table 3.

It can be concluded from the trends of the plots in Figure 8 that the effect of surface tension on wave celerity (for the range of operational conditions under consideration) could not be noticed. Almost all points follow the same trend. The scattered data points are mainly for air–water–glycerin–salt which has a much higher viscosity.

Wave frequency

Wave frequency at different pipe inclination angles is shown in Figure 9. Wave frequency increases with increasing superficial gas velocity. The increase in the superficial liquid velocity results in an increase in the wave frequency. At low V_{SL} (Cases 1–5, V_{SL} = 0.0035 m/s), there is a slight increase in the frequency at high V_{SG} for angles between 10° and 60°. It seems that there is no inclination effect on wave frequency at low V_{SG}.

A relationship between the Strouhal number (dimensionless wave frequency) and the Lockhart–Martinelli number, *X**, has been proposed by Azzopardi[24] for disturbance waves. Figure 10 shows all present work data and data from Mantilla.[19] As suggested by Mantilla[19] for his results only data for V_{SG} >20 m/s in the 2-in. pipe and V_{SG} > 10 m/s in the 0.1524 m pipe were used (annular flow beyond the onset of entrainment) show a linear relationship when plotted on log–log coordinates. Most of the data have similar behavior. The scattered points are mainly for the case of air–water–glycerin–salt of Mantilla's data and at low inclination angles (0°, 10°, and 20°) from the present work at *X** = 0.026.

There seems to be no inclination effect on the Strouhal number except that the low inclination angle data points start to deviate from the straight line at the highest value of *X** and few points for the case of air–water–glycerin–salt data. The trend of *St*–*X** curve is in line with the results of Geraci

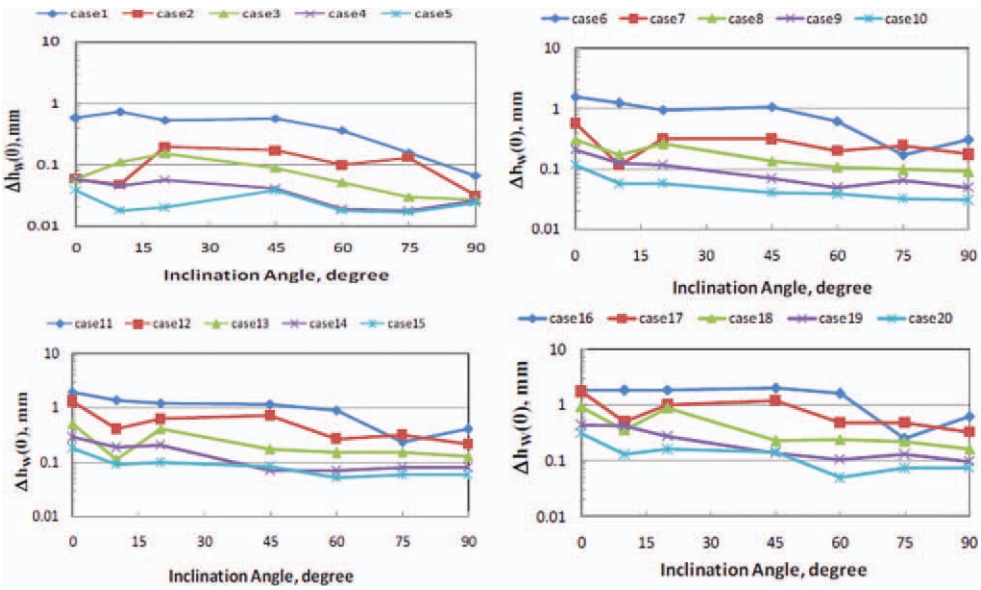

Figure 11. Variation of wave amplitude with pipe inclination angles (cases are shown in Table 1).

[Color figure can be viewed in the online issue, which is available at wileyonlinelibrary.com.]

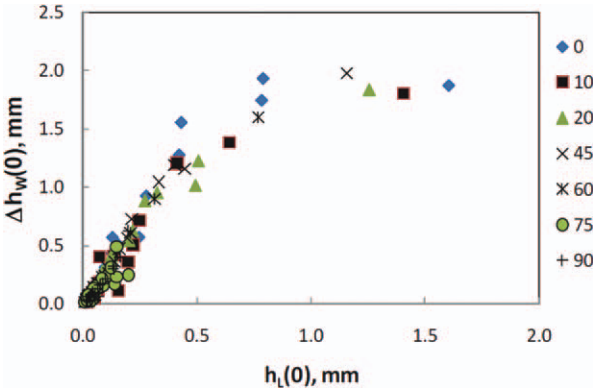

Figure 12. Wave amplitude as a function of liquid film thickness at the bottom of the pipe for all operational conditions.

[Color figure can be viewed in the online issue, which is available at wileyonlinelibrary.com.]

et al.[5,25–27] The Strouhal number can be correlated reasonably for all inclination angles as

$$St = 1.1X^{*-0.93} \tag{5}$$

where Strouhal number is defined as $St = fD/V_{SL}$. f is the wave frequency in Hz, D is the pipe diameter, and V_{SL} is the superficial liquid velocity.

Wave amplitude

Wave amplitude and liquid film thickness are strongly dependent parameters. The wave amplitude and liquid film thickness have an opposite behavior compared with wave celerity with respect to the superficial gas velocity. As superficial gas velocity increases, wave amplitude and average film thickness decrease as the film evenly distributes around the pipe. Similarly, increasing the inclination angle promotes the symmetry of the film, decreasing the average film thickness at the bottom of the pipe, $h_L(0)$, and the wave amplitude, $\Delta h_W(0)$ (see Figure 11).

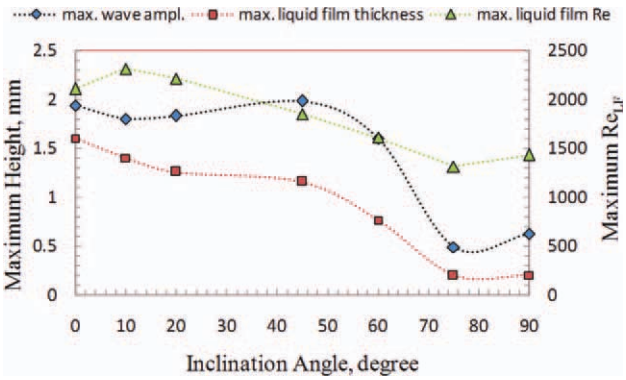

Figure 13. Maximum wave amplitude, liquid film thickness at the bottom of the pipe, and maximum liquid film Reynolds number variation with pipe inclination angle.

[Color figure can be viewed in the online issue, which is available at wileyonlinelibrary.com.]

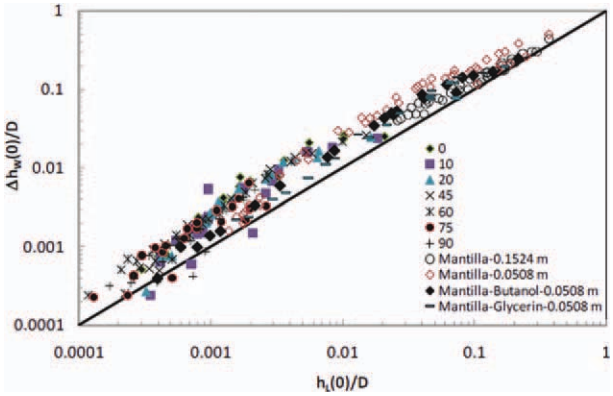

Figure 14. Normalized wave amplitude variation with the normalized liquid film at the bottom of the pipe.

[Color figure can be viewed in the online issue, which is available at wileyonlinelibrary.com.]

Figure 12 shows a very interesting relationship between wave amplitude and the liquid film thickness at the bottom of the pipe. For all operational conditions, the wave amplitude has similar behavior when plotted vs. the liquid film thickness at the bottom of the pipe.

The inclination effects are clear in which the wave amplitude, $\Delta h_W(0)$, for the same range of V_{SL} and V_{SG} could not match the same liquid film thickness at the bottom of the pipe, $h_L(0)$, for all angles of inclination. Wave amplitude and liquid film thickness reach higher values at lower inclination angles than at higher inclination angles for the same operational conditions. Figure 13 shows the variations in the maximum liquid film thickness and maximum wave amplitude points with the angle of inclinations. On the same figure, a plot of liquid film Reynolds number, Re_{LF}, which will be explained later, is also presented. Maximum liquid film thickness, $h_L(0)$, and Reynolds number, Re_{LF}, decrease with increasing the pipe inclination angles. The decrease in the maximum liquid film thickness, $h_L(0)$, and the maximum wave amplitude, $\Delta h_W(0)$, is steeper after 45°. However, the maximum value of wave amplitude stays almost constant up to 45° then decreases sharply with increasing the inclination angle.

Figure 14 shows a comparison between the present work data and Mantilla[19] for air and water in different pipe diameters. All plots show similar behavior in which the wave amplitude increases with increasing the liquid film thickness at the bottom of the pipe.

As can be seen in Figure 14, over the studied range of operational conditions, the wave amplitude is mainly function of the film thickness at the bottom of the pipe, regardless of the pipe diameter and fluid properties. The wave amplitude increases with increasing the average liquid film thickness.

Liquid Film Thickness at the Bottom of the Pipe, $h_L(0)$ and Liquid Film Reynolds Number, Re_{LF}

Average liquid film thickness at the bottom of the pipe, $h_L(0)$

As shown in Figure 15, the average liquid film thickness decreases with increasing pipe inclination angles from

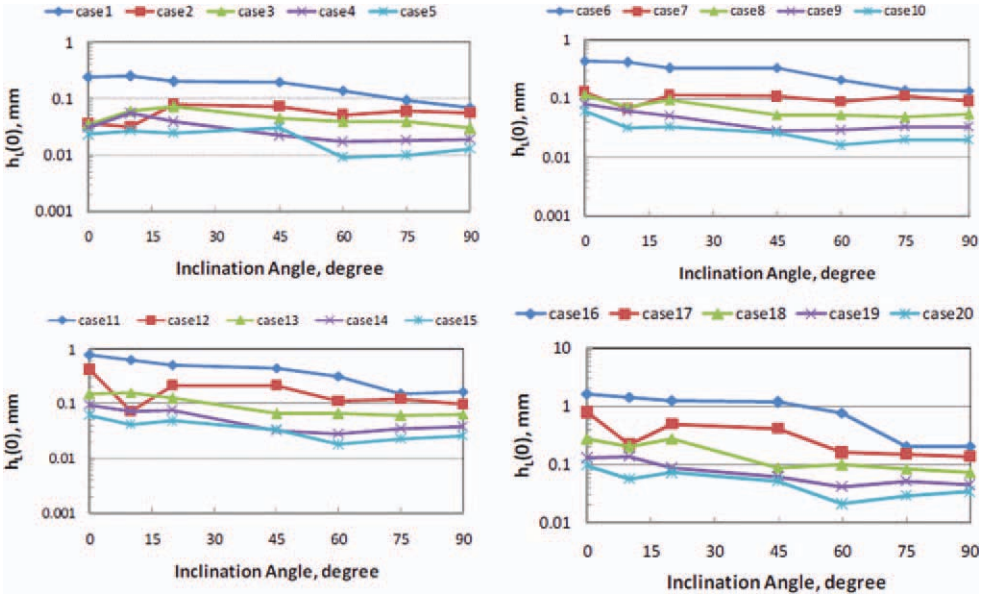

Figure 15. Average liquid film thickness at the bottom of the pipe (units in mm) variations with pipe inclination angles (semi-log scale).

[Color figure can be viewed in the online issue, which is available at wileyonlinelibrary.com.]

horizontal. The film distribution will be symmetric at vertical orientation. Because of the gravitational effect, the increase in pipe inclination promotes the symmetrical distribution of the liquid film around the pipe perimeter. The same result will be achieved with increasing the gas velocity. At the very high gas velocity, the liquid film thickness at the bottom of the pipe does not change much with pipe inclination especially at high angle of inclination (>60°). The average liquid film thickness, $h_L(0)$, increases with increasing superficial liquid velocity.

Liquid film Reynolds number, Re_{LF}

Liquid film Reynolds number, Re_{LF}, is very important parameter for determining the liquid film wall shear stress and the interfacial friction factor in an annular flow.[28] Liquid film Reynolds number can be calculated as in Eq. 6

$$Re_{LF} = \frac{4W_{LF}}{\mu_L \pi D} \tag{6}$$

where W_{LF} is the liquid film mass flow rate (kg/s)

$$W_{LF} = W_L(1 - F_E) \tag{7}$$

where W_L is the liquid mass flow rate ($W_L = \rho_L V_{SL} A_P$), F_E is the fraction of droplet entrainment ($F_E = (W_L - W_{LF})/W_L$), ρ_L is the liquid density, and A_P is the pipe cross-sectional area.

The liquid film Reynolds number can be correlated with X^* as shown in Figure 16. Effects of inclination angle appear after 45° in the form of scattered points from a straight line and only when $X^* > 0.015$. The behavior for inclination angles of 0° to 45° is the same for all range of X^* of this study.

Figure 16 also shows that the liquid film Reynolds number variation with X^* for angle of inclinations 0–45° follows a

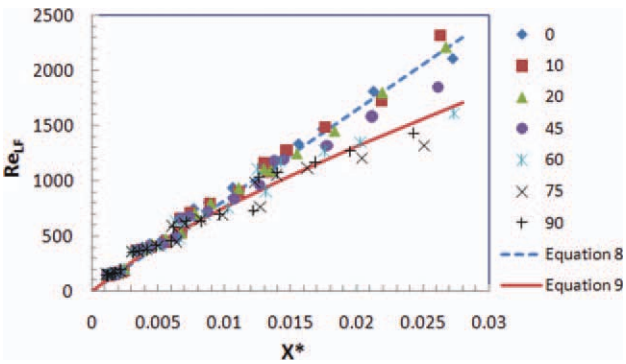

Figure 16. Liquid film Reynolds number variation with X^* for all inclination angles (note inclination angle effect becomes apparent after $X^* = 0.015$).

[Color figure can be viewed in the online issue, which is available at wileyonlinelibrary.com.]

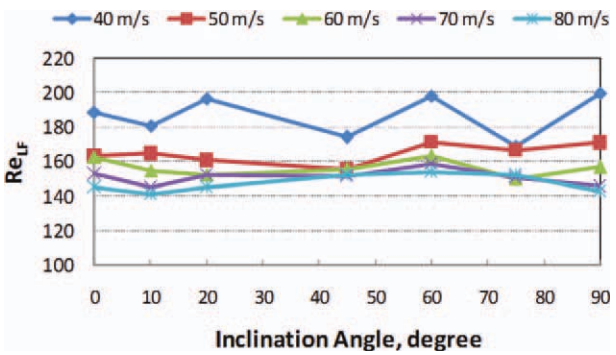

Figure 17. Liquid film Reynolds number variation with pipe inclination at V_{SL} = 0.0035 m/s (legends are V_{SG} in m/s).

[Color figure can be viewed in the online issue, which is available at wileyonlinelibrary.com.]

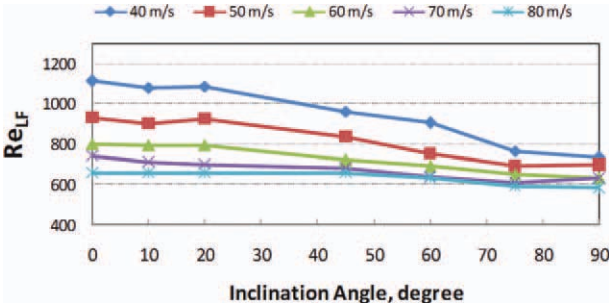

Figure 18. Liquid film Reynolds number variation with pipe inclination at V_{SL} = 0.02 m/s (legends are V_{SG} in m/s).

[Color figure can be viewed in the online issue, which is available at wileyonlinelibrary.com.]

straight line. The liquid film Reynolds number for inclination angles of 0–45° can be well correlated by the straight line equation shown below (the R^2 value for this fit is 0.983)

$$Re_{LF} = 82,331X^* \tag{8}$$

Re_{LF} deviates from the straight line of Eq. 8 for values of $X^* > 0.015$. For angles 60–90°, the liquid film Reynolds number variation with X^*, which is shown in Figure 16, can be well correlated by the power trend line of the form (the R^2 value for this fit is 0.975)

$$Re_{LF} = 28,233X^{*0.785} \tag{9}$$

Figures 17–19 show the variation with pipe inclination angles at certain superficial gas and liquid velocities. At low V_{SL}, the variation of Re_{LF} is not significant with pipe inclination. However, as the V_{SL} increases the effect of pipe inclination on the Re_{LF} is pronounced specially at low superficial gas velocities. At the highest V_{SG}, the effect of pipe inclination on Re_{LF} is not very significant.

Figures 20 shows very interesting behavior of Re_{LF} variation with X^*. Re_{LF} variation with X^* is less sensitive to the pipe diameter. Re_{LF} is not sensitive to the surface tension. However, Re_{LF} is very sensitive to the viscosity

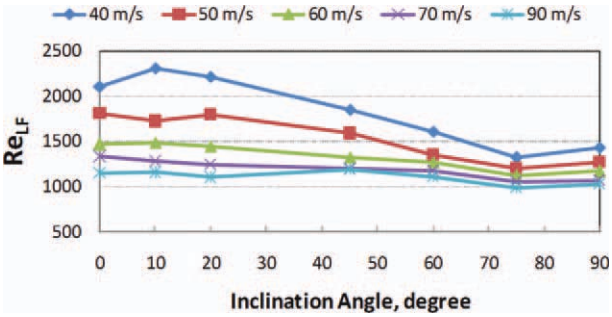

Figure 19. Liquid film Reynolds number variation with pipe inclination at V_{SL} = 0.04 m/s (legends are V_{SG} in m/s).

[Color figure can be viewed in the online issue, which is available at wileyonlinelibrary.com.]

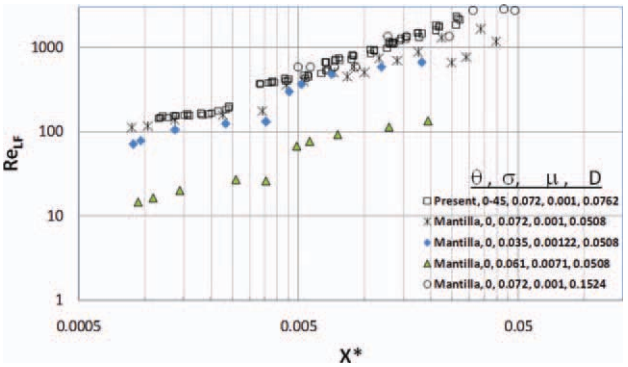

Figure 20. Variation of liquid film Reynolds number with X^* in different pipes, with different surface tension and viscosity (figure's legends are inclination angle, θ, in degree; surface tension, σ, in N/m; dynamic viscosity, μ, in Pa s; and pipe diameter, D, in m).

[Color figure can be viewed in the online issue, which is available at wileyonlinelibrary.com.]

of the flowing liquid. The Re_{LF} is low at higher liquid viscosity.

Liquid Film Velocity, V_{LF}

Liquid film area was estimated from the measurement of the liquid film height at five locations (0°, 45°, 90°, and 180° from the bottom of the pipe) as shown in Figure 21. The half of the film can be unfolded to form a trapezoidal shape as shown in Figure 21.

The arc length between the five measured locations is L_0, L_1, L_2, L_3, which are equals, and can be calculated from

$$L_0 = L_1 = L_2 = L_3 = \frac{D}{2}\frac{45\pi}{180} \tag{10}$$

However, the liquid film internal side arc lengths are not necessarily equals ($l_0 \neq l_1 \neq l_2 \neq l_3$) as the inner side is not absolutely circle, Thus

$$\alpha_1 = \sin^{-1}\left(\frac{h_0 - h_1}{L_1}\right) \tag{11}$$

$$l_0 = L_0\cos(\alpha_1) \tag{12}$$

Then, A_0 is the area of the trapezoid that can be calculated as

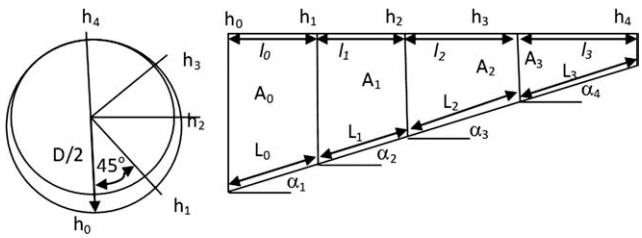

Figure 21. Liquid film measurement locations and distribution of the unfolded liquid film area.

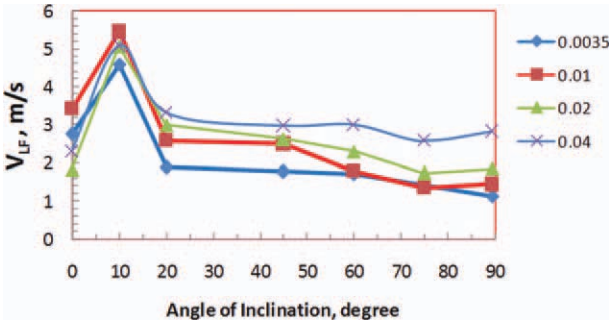

Figure 22. Variation of the liquid film velocity with inclination angle at V_{SG} = 50 m/s (legends are V_{SL} in m/s).

[Color figure can be viewed in the online issue, which is available at wileyonlinelibrary.com.]

$$A_0 = \left(\frac{h_0 + h_1}{2}\right) l_0 \tag{13}$$

Similarly, A_1, A_2, and A_3 are obtained.

Thus, the total liquid film area will be $A_{LF} = 2 \times (A_0 + A_1 + A_2 + A_3)$ and the liquid film velocity will be $V_{LF} = W_{LF}/(\rho_L A_{LF})$. The hydraulic diameter of the liquid film and Reynolds number can be calculated as

$$D_{h_{LF}} = \frac{4A_{LF}}{\pi D}; \qquad Re_{LF} = \frac{\rho_L V_{LF} D_{h_{LF}}}{\mu_L} \tag{14}$$

Plots of V_{LF} variation with pipe inclinations are illustrated in Figures 22–24. Liquid film velocity is a function of the superficial liquid and gas velocities and the pipe inclination angle. V_{LF} increases with increasing the V_{SL} and V_{SG}. The plots of the V_{LF} vs. the inclination angle show a peak value for V_{LF} at certain angle for certain condition. This peak is shifted toward the higher angles as the superficial gas velocity increases.

Concluding Remarks

Wave characteristics are very crucial for understanding and modeling of any annular flow. Pipe inclination effects on wave characteristics have been studied in this article.

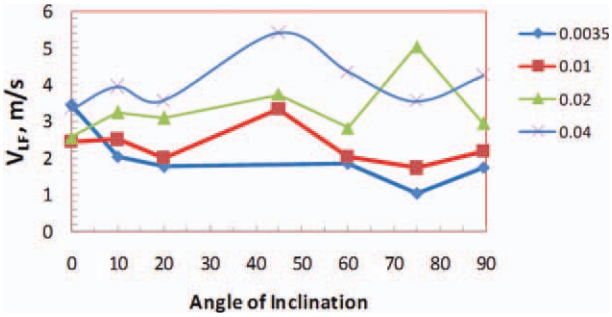

Figure 23. Liquid film velocity variation with pipe inclination at V_{SG} = 60 m/s (legends are V_{SL} in m/s).

[Color figure can be viewed in the online issue, which is available at wileyonlinelibrary.com.]

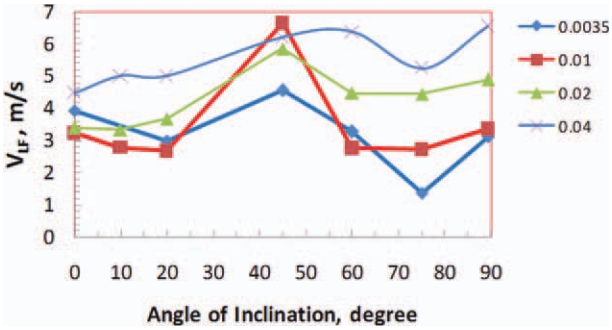

Figure 24. Liquid film velocity variation at V_{SG} = 70 m/s (legends are V_{SL} in m/s).

[Color figure can be viewed in the online issue, which is available at wileyonlinelibrary.com.]

Measurements of wave characteristics have been conducted in a 0.0762 m ID pipe and compared with measurement of Mantilla[19] for different pipe diameter and surface tension.

Most interestingly, wave amplitude may be presented as a function of liquid film thickness at the bottom of the pipe for any pipe diameter, surface tension, and viscosity. Wave amplitude increases sharply with increasing the liquid film thickness at the bottom of the pipe.

Liquid film Reynolds number for horizontal and low inclination angle cases is strongly dependent on the modified Lockhart–Martinelli parameter X^*. Re_{LF} for different surface tension, viscosity, and pipe diameter is presented in this work as a function of X^*. Increasing X^* will increase Re_{LF}. Re_{LF} is less sensitive to the change in pipe diameter and surface tension and very sensitive to the change in liquid viscosity.

Dimensionless wave celerity (C/V_{SL}) is also well correlated with X^*. Increasing X^* will decrease the C/V_{SL}. The grouping of low inclination and higher inclination angles was clearly noticed on the plots of C/V_{SL} vs. X^*. The low inclination angles have higher C/V_{SL} than the higher inclination angles. The effect of surface tension, viscosity, and pipe diameter was presented in this work. The effect of pipe diameter of the behavior of C/V_{SL} vs. X^* was insignificant. The effect of the surface tension was also insignificant. The effect of liquid viscosity was pronounced only at lower values of X^*. The dimensionless wave frequency (Strouhal number) is well correlated with X^*. Strouhal number for different pipe diameter, viscosity, and surface tension at different inclination angles is presented in this article as a function of X^*. The larger the X^*, the smaller the Strouhal number.

Maximum value of liquid Reynolds number and liquid film thickness at the bottom of the pipe decreases with increasing the angle of inclination. The maximum value of the wave amplitude decreases sharply with increasing the angle of inclination only at higher inclination angles (large than 45°).

Literature Cited

1. Al-Sarkhi A, Hanratty TJ. Effect of pipe diameter on the performance of drag-reducing polymers in annular gas–liquid flows. *Trans IChemE: Chem Eng Res Des*. 2001;79(Part A):402–408.
2. Geraci G, Azzopardi BJ, van Maanen HRE. Inclination effects on circumferential film flow distribution in annular gas/liquid flows. *AIChE J*. 2007;53:1144–1150.

3. Azzopardi BJ, Whalley PB. Artificial waves in annular two-phase flow. ASME Winter Annual Meeting, Chicago, IL, November 16–21, 1980.
4. Sutharshan B, Kawaji M, Ousaka A. Measurement of circumferential and axial liquid film velocities in horizontal annular flow. *Int J Multiphase Flow*. 1995;21:193–206.
5. Geraci G, Azzopardi BJ, van Maanen HRE. Effect of inclination on circumferential film thickness variation in annular gas/liquid flow. *Chem Eng Sci*. 2007;62:3032–3042.
6. Woodmansee DE. Atomization from a flowing horizontal water film by a parallel air flow, Ph.D. Dissertation. University of Illinois at Urbana-Champaign, 1968.
7. Ishii M, Grolmes MA. Inception criteria for droplet entrainment in two-phase concurrent film flow. *AlChE J*. 1975;21:308–318.
8. Lighthill MJ, Whitham GB. On kinematic waves. I. Flood movement in long rivers. *Proc R Soc Lond Ser A: Math Phys Sci*. 1955; 229:281–345.
9. Wallis GB. *One Dimensional Two-Phase Flow*. New York: McGraw-Hill, 1969.
10. Andreussi P, Asali JC, Hanratty TJ. Initiation of roll waves in gas–liquid flows. *AIChE J*. 1985;31:119–126.
11. Andritsos N. Effect of pipe diameter and liquid viscosity on horizontal stratified flow, Ph.D. Dissertation. University of Illinois at Urbana-Champaign, 1986.
12. Bruno K, McCready MJ. Origin of roll waves in horizontal gas–liquid flows. *AIChE J*. 1988;34:1431–1440.
13. Barnea D, Taitel Y. Kelvin–Helmholtz stability criteria for stratified flow: viscous versus non-viscous (inviscid) approaches. *Int J Multiphase Flow*. 1993;19:639–649.
14. Hanratty TJ, Hershman A. Initiation of roll waves. *AIChE J*. 1961;7:488–497.
15. Miya M, Woodmansee DE, Hanratty TJ. A model for roll waves in gas–liquid flow. *Chem Eng Sci*. 1971;26:1915–1931.
16. Watson M. *Wavy stratified flow and the transition to slug flow*. *Proceedings of the 4th International Conference in Multi-phase Flows*, Nice, France, 1989.
17. Pols RM. Waves in separated two-phase flow, Ph.D. Dissertation. The University of Nottingham United Kingdom, 1998.
18. Johnson GW, Nossen J, Bertelsen AF. *A Comparison Between Experimental and Continuous Theoretical Roll Waves in Horizontal and Slightly Inclined Pipes at High Pressure*. Barcelona: BHR Group Multiphase Production Technology, 2005.
19. Mantilla I. Mechanistic modeling of liquid entrainment in gas in horizontal pipes, Ph.D. Dissertation. The University of Tulsa, 2008.
20. Mantilla I, Gomez L, Mohan R, Shoham O, Kouba G, Roberts R. Experimental investigation of liquid entrainment in gas in horizontal pipes. Proceedings of ASME 2009 Fluids Engineering Division Summer Meeting, Vail, Colorado, August 2–5, 2009; FEDSM2009-78420.
21. Magrini K. Liquid entrainment in annular gas–liquid flow in inclined pipes, M.S. Dissertation. The University of Tulsa, 2009.
22. Al-Sarkhi A, Sarica C. Power law correlation for two phase pressure drop of gas/liquid flows in horizontal pipelines. *SPE Proj Fac Const*. 2010;5:176–182; SPE 138516-PA.
23. Lockhart, RW, Martinelli RC. Proposed correlation of data for isothermal two-phase, two-component flow in pipes. *Chem Eng Progr*. 1949;45:39–48.
24. Azzopardi BJ. *Gas–Liquid Flows*. New York: Begell House, Inc., 2006.
25. Fukano T, Ousaka A, Morimoto T, Sekoguchi K. Air-annular two-phase flow in a horizontal tube. *Bull Jpn Soc Mech Eng*. 1983;26: 1387–1395; second report.
26. Jayanti S, Hewitt GF, White SP. Time dependent behaviour of the liquid film in horizontal annular flow. *Int J Multiphase Flow*. 1990;16:1097–1116.
27. Paras SV, Karabelas, AJ. Droplet entrainment and deposition in horizontal annular flow. *Int J Multiphase Flow*. 1991;17:455–468.
28. Henstock WH, Hanratty TJ. The interfacial drag and the height of the wall layer in annular flow. *AIChE J*. 1976;22:990–1000.

Manuscript received Sept. 7, 2010, revision received Feb. 24, 2011, and final revision received Apr. 7, 2011.